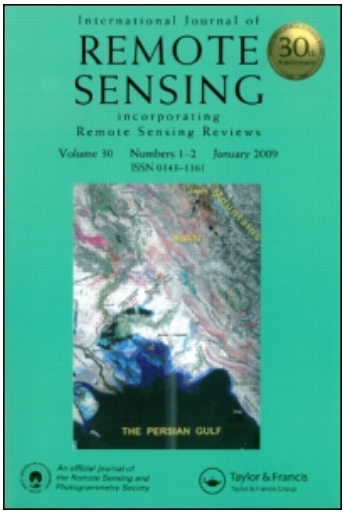

International Journal of Remote Sensing
Publication details, including instructions for authors and subscription information:
http://www.informaworld.com/smpp/title~content=t713722504

Mapping sub-pixel burnt percentage using AVHRR data. Application to the Alcalaten area in Spain

Ana B. Ruescas[a]; Jose A. Sobrino[a]; Yves Julien[a]; Juan C. Jiménez-Muñoz[a]; Guillem Sòria[a]; Victoria Hidalgo[a]; Mariam Atitar[a]; Belen Franch[a]; Juan Cuenca[a]; Cristian Mattar[a]
[a] Imaging Processing Laboratory, Polígono La Coma s/n (46980 Paterna), University of Valencia, Spain

Online publication date: 20 October 2010

To cite this Article Ruescas, Ana B. , Sobrino, Jose A. , Julien, Yves , Jiménez-Muñoz, Juan C. , Sòria, Guillem , Hidalgo, Victoria , Atitar, Mariam , Franch, Belen , Cuenca, Juan and Mattar, Cristian(2010) 'Mapping sub-pixel burnt percentage using AVHRR data. Application to the Alcalaten area in Spain', International Journal of Remote Sensing, 31: 20, 5315 — 5330

To link to this Article: DOI: 10.1080/01431160903369592
URL: http://dx.doi.org/10.1080/01431160903369592

International Journal of Remote Sensing
Vol. 31, No. 20, 20 October 2010, 5315–5330

Taylor & Francis
Taylor & Francis Group

Mapping sub-pixel burnt percentage using AVHRR data. Application to the Alcalaten area in Spain

ANA B. RUESCAS*, JOSE A. SOBRINO, YVES JULIEN, JUAN C. JIMÉNEZ-MUÑOZ, GUILLEM SÒRIA, VICTORIA HIDALGO, MARIAM ATITAR, BELEN FRANCH, JUAN CUENCA and CRISTIAN MATTAR

Imaging Processing Laboratory, Polígono La Coma s/n (46980 Paterna), University of Valencia, Spain

(*Received 28 April 2008; in final form 15 March 2009*)

The purpose of this work is to estimate at sub-pixel scale the percentage of burnt land using the Advanced Very High Resolution Radiometer (AVHRR) through a simple approach. This methodology is based on multi-temporal spectral mixture analysis (MSMA), which uses a normalized difference vegetation index (NDVI) and a land-surface temperature (LST) image as input bands. The area of study is located in the Alcalaten region in Castellon (Spain), a typical semi-arid Mediterranean region. The results have shown an extension of approximately 55 km^2 affected by fire, which is only 5% lower than the statistic reports provided by the Environmental Ministry of Spain. Finally, we include a map of the area showing the percentage of estimated burnt area per pixel and its associated uncertainties. The map was validated through supervised classification of an Airborne Hyperspectral Sensor (AHS) image taken on 27 September 2007. Results have a high accuracy, with a mean error of 6.5%.

1. Introduction

After a fire occurs, an estimation of the burnt area must be carried out as soon as possible in order to quantify the damage and to establish the economic losses. This kind of information is relevant for insurance companies and governments, who must cover expenses to compensate people for their losses and to start reforestation.

The aim of this study is to show and evaluate a simple methodology based on spectral mixture analysis (SMA) using low-spatial-resolution sensors such as the Advanced Very High Resolution Radiometer (AVHRR) of the National Oceanic and Atmospheric Administration. These images were used to estimate and map the sub-pixel burnt area a short time after the event. AVHRR images have been widely used in mapping burnt areas on a global and regional scale (Pozo *et al*. 1997, Barbosa *et al*. 1998, 1999, Sousa *et al*. 2003, Quintano *et al*. 2006, Chuvieco *et al.* 2008), and these were easily available immediately after the fire.

The methodology presented here made used of the normalized difference vegetation index (NDVI) in order to obtain pure pixels (endmembers) to be used in a multi-temporal spectral mixture analysis (MSMA) model (Song 2005). For the mixture analysis itself, we used the NDVI image and thermal infrared data, which was included by means of a land-surface temperature (LST) image obtained with the

*Corresponding author. Email: bruescas@uv.es

International Journal of Remote Sensing
ISSN 0143-1161 print/ISSN 1366-5901 online
http://www.tandf.co.uk/journals
DOI: 10.1080/01431160903369592

application of an LST algorithm (Gillespie 1992, Sobrino and Raissouni 2000). LST has rarely been used to estimate burnt-area extension, although we think that including it in the SMA may increase the accuracy of the estimation and complement information of bands 1 and 2, which are summarized in the NDVI parameter. NDVI and LST have been shown to present a linear correlation (Nemani *et al.* 1993, Hope *et al*. 2005, Yue *et al*. 2007) and to be related to surface moisture status (Sandholt *et al.* 2002). Therefore, their use in a linear spectral model seems adequate for estimation of burnt area.

In AVHRR imagery, the scale of spatial variation in land cover is generally finer than the ground-resolution element associated with the pixel, which means that most AVHRR pixel values represent a sample of a mixture of different land-cover classes. This is specifically the case for semi-arid regions where the distribution of soil and vegetation is highly variable. There are several techniques for classifying sub-pixel variation in land cover, such as artificial neural networks (ANNs) (Carpenter *et al.* 1999), supervised classifications or spectral mixture modelling (Gillespie 1992, Elmore *et al.* 2000, Theresia *et al.* 2003). Atkinson *et al*. (1997) evaluated three different techniques in terms of the amount of information extracted, the accuracy of that information and the ease of implementation: fuzzy *c*-means classifiers, ANNs and SMA. They concluded that the ANN technique was superior to the other two in terms of the information provided and its accuracy. However, in terms of implementation, the fuzzy *c*-means classification and the mixture analysis were easier to apply because they do not require so much training data and previous knowledge of the area. If an accurate method for selecting pure endmember spectra was developed, the accuracy of the SMA would increase and that would make the technique a simpler and less time-consuming way of sub-pixel classification. Here, we have selected the endmembers using both visual and semi-automated approaches in order to define more suitable representations of the study area.

Results were validated by comparing the calculated area with the statistic reports provided by the Environmental Ministry of Spain (MMA). An image of the percentage of burnt area per pixel is also presented and validated with an Airborne Hyperspectral Sensor (AHS) image taken a few days after the fire, with greater than 90% accuracy when considering a supervised classification of the AHS as reference data.

The area of study (see figure 1) is located in L'Alcalaten County in Castellon (Spain), a semi-arid Mediterranean region, with coordinates 40° 08′ N, 0° 10′ W in an approximate central point. This area was covered mainly by shrubs and fruit-tree fields, with a small part covered by pine and deciduous-tree forests. In the province of Castellon, in 2007, around 78 km^2 were affected by fire (14 km^2 of trees, 63.5 km^2 of shrubs and 50 km^2 of grassland). Most of the area affected by fire was burnt in only one event, the fire in L'Alcalaten County, which started on 28 August 2007 and ended on 31 August 2007. Of all the area that burnt in the Comunidad Valenciana in 2007, 95% of it happened during those 4 days.

2. Data and methodology

2.1 *Data*

We employed here three AVHRR images that were captured and archived with a high-resolution picture transmission (HRPT) antenna and reception system, owned by the Imaging Processing Laboratory of the University of Valencia. One was taken

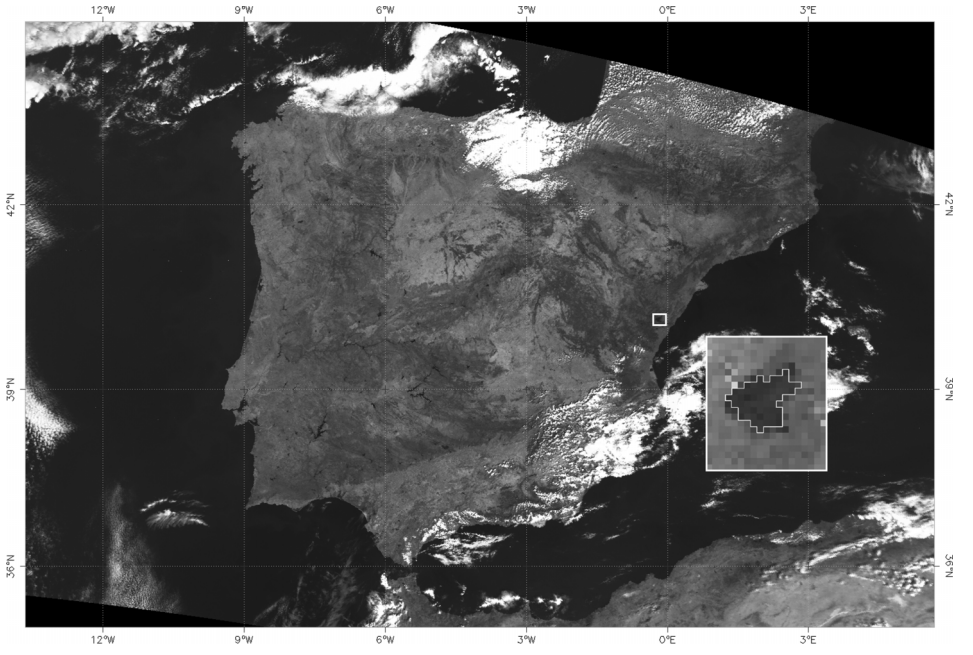

Figure 1. Location of study area within the Iberian Peninsula AVHRR image.

3 days before the fire event (28 August 2007), another one 4 days after the fire (4 September 2007) and the last one 9 days afterwards, when the fire was officially declared extinct (9 September 2007). The images were radiometrically corrected and the applied georeference resulted in a root mean square error less than one pixel.

We use the statistics report created by the Department of Defence Against Forest Fires of the General Secretary for Biodiversity depending on the Environmental Ministry of Spain (*Area de Defensa contra los Fuegos Forestales de la Dirección General para la Biodiversidad del Ministerio de Medio Ambiente*, MMA 2008). Statistics were used as validation data for the calculation of the total burnt area. This Department used the Moderate Resolution Imaging Spectroradiometer (MODIS) sensor with a spatial resolution of 250 × 250 m for detecting and quantifying areas affected by fire. The Department of Defence Against Forest Fires worked in collaboration with the European Commission's Joint Research Centre (Ispra, Italy), that also processed Satellite Pour l'Observation de la Terre (SPOT5) data for this case study. Within the classification of vegetation affected by the fire by counties, the MMA could provide us with an estimation of the area affected per vegetation class in the study area, which we took into account for validation purposes. Total burnt area was estimated to be around 57 km^2 (Ministerio de Medio Ambiente 2008).

Furthermore, we also used an AHS image to validate the percentage of burnt area estimated by pixel within the AVHRR scene. The AHS image was taken on 27 September 2007, thanks to the National Institute of Aeronautic Techniques (*Instituto Nacional de Técnica Aeroespacial*) airborne facility. The flight was part of the CarboEurope, FLEX and Sentinel project (CEFLES) funded by the European Space Agency (ESA). The area imaged by the AHS does not cover the total burnt area, but only its central location, the zone where the fire began near Useres village (0.17° W and 40.17°

N). The original spatial resolution of the AHS is 6×6 m, and its spectral resolution in the visible covers from 0.45 to 1.002 μm in 20 bands of 0.30 μm spectral resolution.

2.2 *Methodology*

2.2.1 Total burnt-area extension. The first step for the application of the proposed method was to define the whole area affected by the fire in the AVHRR scenes, where we chose the endmembers. In this way, we could avoid taking into account the rest of the area included in the satellite images. After eliminating pixels contaminated by clouds using the filters proposed by Saunders and Kriebel (1998), four approaches were applied to determine that total burnt area. Two of them were simple false-colour compositions, the most frequently used for burning discrimination: the first was a visual approach based on a decorrelation stretch technique that uses channels 1 (0.58–0.68 μm), 2 (0.72–1.1 μm) and 4 (10.3–11.3 μm) of the AVHRR assigned to red, green and blue (RGB) colours, respectively; the second one consisted of a composition based on the calculated difference of the spectral values of channels 1, 2 and 3 (1.57–16.7 μm) of the images before and after the fire event, assigned again to RGB. With both methods, we digitized the area manually and the estimation showed us that nearly 72 km^2 was affected by the fire. The third method consisted of a simple difference between the NDVI images pre- and post-fire, but it was calculated for two different post-fire images, 4 September and 9 September 2007. The total area, again digitizing manually, gave us around 66 km^2 of burnt area estimated with both dates. The fourth and last approach was implemented automatically in Interactive Data Language (IDL), and can be summarized in figure 2 (step 1: determination of the total burnt area). To that end, the NDVI difference between post- and pre-fire images (ΔNDVI) was calculated to identify a first estimate of the burnt area, being the area for which ΔNDVI was lower than the average of the ΔNDVI image. This operation was iterated by calculating a new NDVI difference between post- and pre-fire images from which the burnt area has been excluded. This procedure aimed at selecting as burnt pixel the ones for which the NDVI value had decreased between the two acquisitions, through considering eventual changes in observation conditions, mainly due to sun–target–sensor geometry and atmospheric contamination. Three iterations were needed to reach stability of the burnt-area extension. The reason for this iterative process is that the NDVI difference between pre- and post-fire conditions (excluding the burnt area) depends on the extension of the burnt area, and therefore has to be estimated iteratively until the extent of the burnt area remains unchanged. The date of the post-fire image was chosen to be 9 September 2007. A surrounding unburnt area was also identified by subtracting the burnt area from a dilatation of the burnt area. Later on we compensated differences in acquisition conditions, which consisted of the addition of a constant for each channel of the pre-fire image. This constant was calculated as the average of the difference between the values of the corresponding channels in the post- and pre-fire images over the surrounding unburnt area. This could be considered as a local correction of the differences in image acquisition between the two considered dates. The total area affected by the fire with this fourth automatic method was 77.44 km^2, including surrounding areas. Figure 3 shows the area estimated for each method. We decided not to draw the digitized vector of the burnt area in order to make visible the implicit subjectivity in the digitizing process from a qualitative assessment.

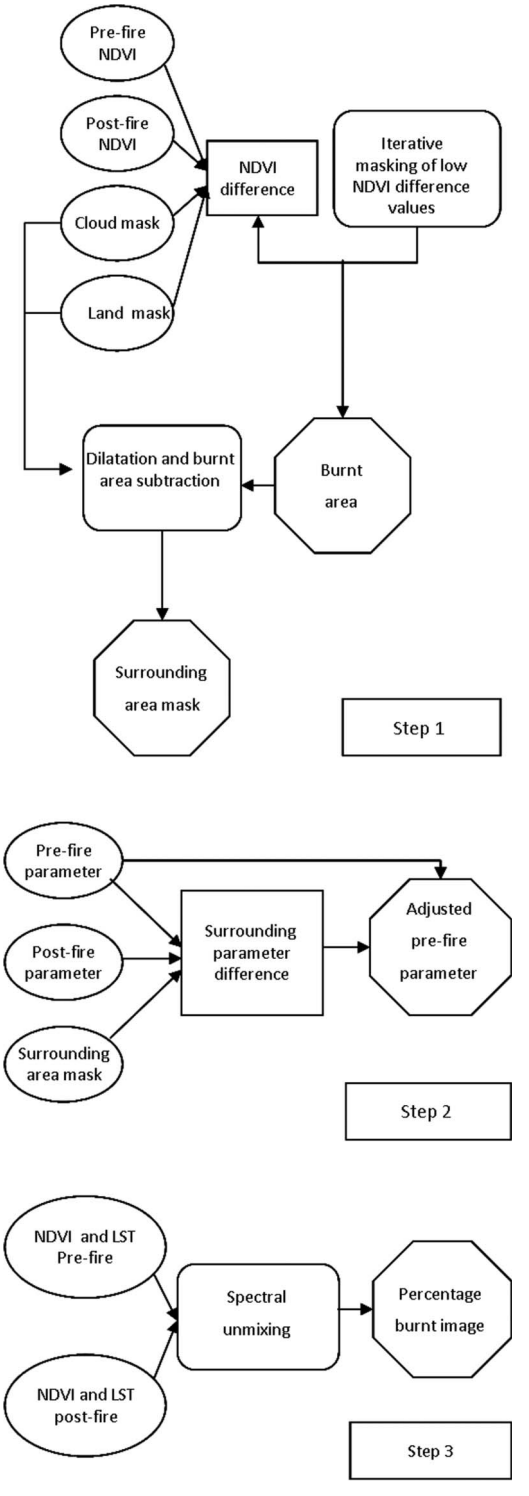

Figure 2. Methodology chart. Step 1: total burnt-area extension first estimation, step 2: pre- and post-fire image observation conditions matching for endmember selection and step 3: sub-pixel burnt percentage estimation.

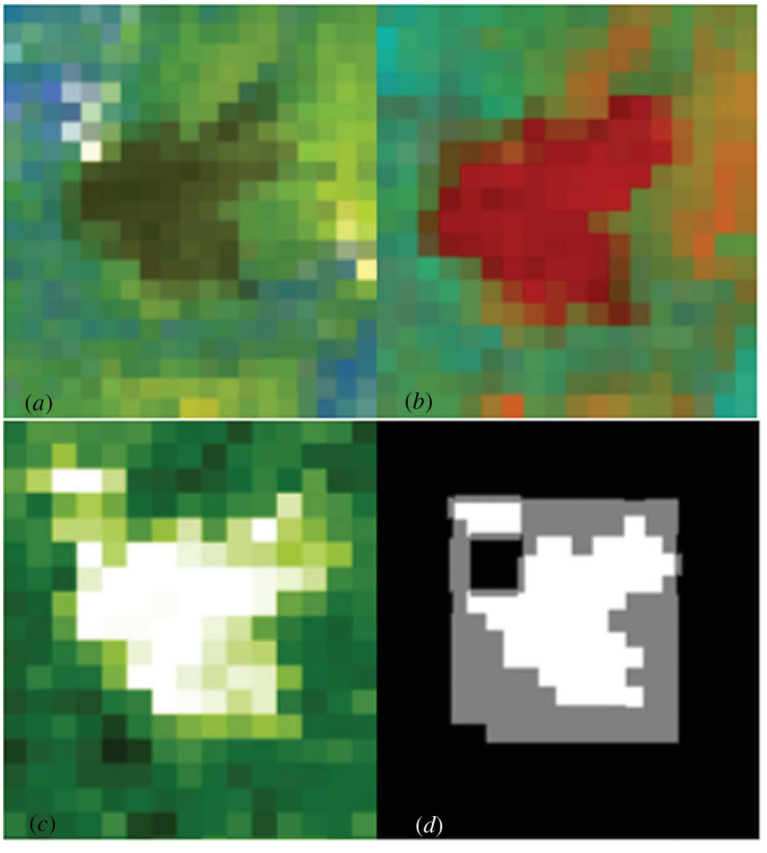

Figure 3. Burnt-area estimation with four methods (pre-fire image: 28 August 2007; post-fire image: 9 September 2007): (*a*) RGB-123 on (*b*) decorrelation stretch RGB-124, (*c*) NDVI differences and (*d*) automatic detection (40° 08′ N, 0° 10′ W central pixel).

These four results cover a larger extent of area affected by the fire than the reference span calculated by the MMA of around 57 km^2, but they were a necessary approximation in order to develop the SMA method with the total assurance of including all the area that could have been affected by the fire, but at the same time avoiding the area that has definitely not been affected. We then used the pixels of this limited area to select endmembers.

2.2.2 Endmember selection. There are different procedures for choosing endmembers, the simplest technique being to locate pure endmembers using appropriate ancillary information such as ground data. For low-resolution imagery, some other methods for selecting endmembers are: using reflectance images (Atkinson *et al.* 1997), calculating principal components (Cross *et al.* 1991), applying geometric-optical modelling (Asner *et al.* 1997) or using regression techniques (Holben and Shimabukuro 1993).

We extracted endmembers spectral signatures from the satellite data, called the image endmembers, using the NDVI calculated from the reflectance images. The NDVI has shown a high sensitivity to the presence of vegetation, and it has been

frequently used within SMA (Kerdiles and Grondona 1995, Defries *et al.* 2000). Linear mixing predominates the non-linear interaction for NDVI values in mixed pixels. Appropriate endmembers must define a coherent set of spectra representative of physical components of the surface (Coppin *et al.* 2004). This is the most critical stage of the SMA method because the AVHRR has a spatial resolution of 1.1 × 1.1 km, and the endmembers should represent a unique type of cover. We decided to start selecting only two endmembers, one representative of pure burnt area (100% burnt) and the other one representative of unaffected vegetation inside the burnt area. Due to the fact that there is no unique and infallible method for discriminating pure pixels, we tried different methods for endmember selection. The 100% burnt pixel was fixed and always the same for all tested methods, and its location was known and verified by fieldwork. The vegetation endmember varied within each of the four following models. First, we considered only one pixel of vegetation representative of the whole area affected by the fire. This single pixel was always taken from the pre-fire image and corresponds to a low NDVI value in the post-fire image, in order to be completely sure that it had been affected by the fire. We tested different values of NDVI (see table 1), the maximum NDVI in the first test, the minimum NDVI in the second test and the mean NDVI for a third test, averaging minimum and maximum values. The fourth test consisted of selecting the NDVI value of each pixel from the pre-fire image as the vegetation endmember; to be precise, we did not consider a single NDVI value for the whole burnt area, but a different value for every pixel inside the burnt area. The atmospheric and illumination changes between pre-fire and post-fire images were accounted for by adding the averaged NDVI difference (AVGDIF) around the burnt area before and after fire (NDVI + AVGDIF in table 1). In other words, this last method was implemented considering each pixel as an independent endmember that could be used along with the burnt endmember as inputs in the spectral unmixing calculation. This method was designed in order to avoid the attribution of artificially high NDVI values for pre-fire vegetation when the corresponding pixel may not have shown such a high vegetation density. Therefore, the pre-fire NDVI value was adjusted to post-fire observation conditions by matching the pre- and post-fire NDVI averages in the area surrounding the fire scar (see figure 2, step 2). Then, for each pixel, the adjusted pre-fire NDVI value was considered as the unburnt endmember, considered as a local and reliable pre-fire condition. This fourth test was chosen as the most accurate because, when calculating again the total burnt area extracted using those four models for selecting endmembers, the values of total burnt area were close to the number given by the MMA (±54 km^2). The area was

Table 1. Results of the MSMA models.

Date	Vegetation endmember (NDVI component)	Area (km^2)
9 September 2007	maximum NDVI	57
9 September 2007	mean NDVI	34
9 September 2007	minimum NDVI	23
9 September 2007	NDVI + AVGDIF	53
4 September 2007	maximum NDVI	42
4 September 2007	mean NDVI	39
4 September 2007	minimum NDVI	20
4 September 2007	NDVI + AVGDIF	55

calculated automatically using IDL procedure script. Results are shown in table 1 using two different post-fire images, as explained above. The fourth of the tested methods (NDVI + AVGDIF) provides the estimation closest to the official burnt area with a good agreement for both post-fire dates.

2.2.3 Sub-pixel burnt percentage using SMA. In this paper, we use a variation of the SMA technique, which assumes that pixel values are linear combinations of reflectance from a limited set of constituent's elements or endmembers. The essential assumptions for SMA are that a landscape is composed of a limited number of fundamental components, that the spectral signature for each component is spatially constant and that the remotely sensed signal of a pixel is linearly related to fractions of the endmember used. In SMA, the spectral properties of a pixel are modelled as a linear combination of endmember spectra weighted by the percent ground coverage of each endmember. The SMA applied here uses images from different dates, and therefore it should be considered an MSMA. Good results have been obtained in studies related to land-cover change detection with this technique (Roberts *et al.* 1998). We applied an MSMA model using the endmembers explained in section 2.2.2. and, as input bands, the NDVI and the LST values extracted from the spectral images.

The applied LST algorithm uses channels 4 and 5 of the AVHRR, the calculated mean effective emissivity (ε), the emissivity difference ($\Delta\varepsilon$) and the water vapour content (g cm^{-2}) (Sobrino and Raissouni 2000). The algorithm has the general form

$$\begin{aligned}\mathrm{LST} = {} & T_{11} + 1.40(T_{11} - T_{12}) + 0.32(T_{11} - T_{12})^2 + 0.83 + (57 + 5W)(1 - \varepsilon) \\ & + (161 + 30W)\Delta\varepsilon, \end{aligned} \tag{1}$$

where T_{11} and T_{12} are the at-sensor brightness temperatures (in K) for the two thermal infrared AVHRR channels 4 and 5, ε is the mean emissivity, $\varepsilon = 0.5\,(\varepsilon_i + \varepsilon_j)$, $\Delta\varepsilon$ is the emissivity difference, $\Delta\varepsilon = (\varepsilon_i - \varepsilon_j)$ and W is the atmospheric water vapour content (in g cm^{-2}). The emissivities for each thermal band of the AVHRR (ε_i and ε_j) depend on NDVI thresholds and vary with the study area, so they must be calculated using the NDVI information extracted from the image (for more details, see Sobrino and Raissouni (2000)).

We have applied this new methodology considering the initial day of fire and two different final dates, as shown in table 1, in order to test the variability of the results depending on how many days had passed after the fire event. We decided to proceed with two analyses with different end dates to carry out a comparison of the results depending on different atmospheric conditions. In step 3 of figure 2, the flow chart shows the approach followed to obtain the percentage burnt image using the spectral unmixing technique. The unmixing analysis was carried out by inversion of the matrix through singular value decomposition. This inversion was made by setting a burnt pixel percentage of 100% for burnt endmembers and 0% for unburnt endmembers. No image error was obtained. Obviously, fractions of burnt area were set between 0% and 100%, with the fractions of burnt and unburnt areas summing to 100% for each pixel. The whole methodology was implemented using the IDL.

3. Results

A total burnt area of 55 km^2 was estimated on 4 September 2007 and 53 km^2 on 9 September 2007, which agree with the results provided by the MMA of 57 km^2, 4.7 km^2 of trees and 53 km^2 non-trees (MMA 2008). We finally chose the last day

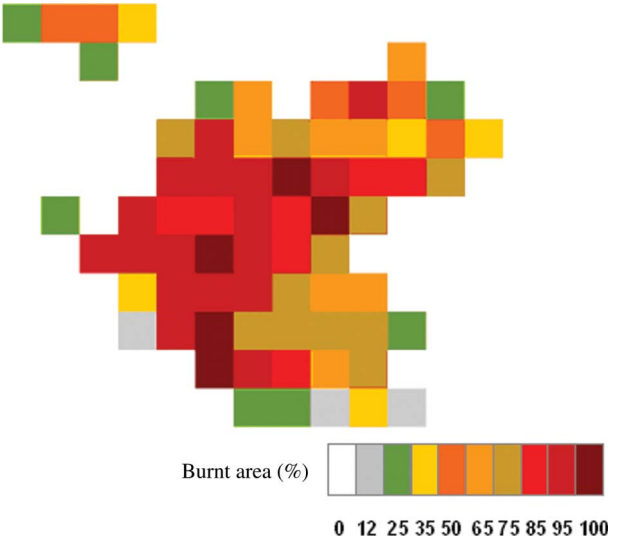

Figure 4. Percentage of burnt area; coordinates of central point 40° 08′ N, 0° 10′ W.

(9 September 2007) as the end date to create and validate the sub-pixel percentage map because it was the official date of the fire extinction from which official statistics were extracted.

A map of the percentage of burnt area per pixel was estimated by the MSMA and it is shown in figure 4. As can be seen in the legend, the percentage of burnt area varies from pixels of areas almost completely burnt (93%) to others less affected by the fire (15%). The mean value for the total area is 66% burnt. The pixels with more vegetation undamaged are located in the margin areas. There is a highly damaged region on the left of the map, which coincides with the steepest mountainous area and corresponds to pixel 2 in the evaluation process with the AHS explained in the next section.

4. The evaluation process

Due to the limited area covered by the AHS, we selected four zones of 1.1 × 1.1 km using coordinates corners from the AVHRR image to simulate four pixels in the AHS image (see figure 5).

These four pixels represent around 7% of the total burnt area. Congalton and Green (1999) estimate a sample of at least 1% of the area to do a proper accuracy assessment. The difference in the spatial resolution of both sensors must be pointed out, as only one AVHRR pixel corresponds to 183 × 183 pixels in the AHS image, and the pixels were delineated using the coordinates corners of the AVHRR pixels. We classified the area inside the AHS pixels using a maximum likelihood classification approach. The training fields of each class of interest were selected within each pixel specifically, using visual interpretation of several band-composition images and visiting the field to check its suitable location. The land-cover classes varied within each pixel depending on the land cover found in it: healthy vegetation (VEG), shadowed vegetation (VEGS), burnt area (BUR), burnt area in shadow (BUS), partly burnt vegetation (VEB), burnt area with small vegetation patches (BUV) and rocks and bare soil (ROC). See figure 6 for pixel classifications.

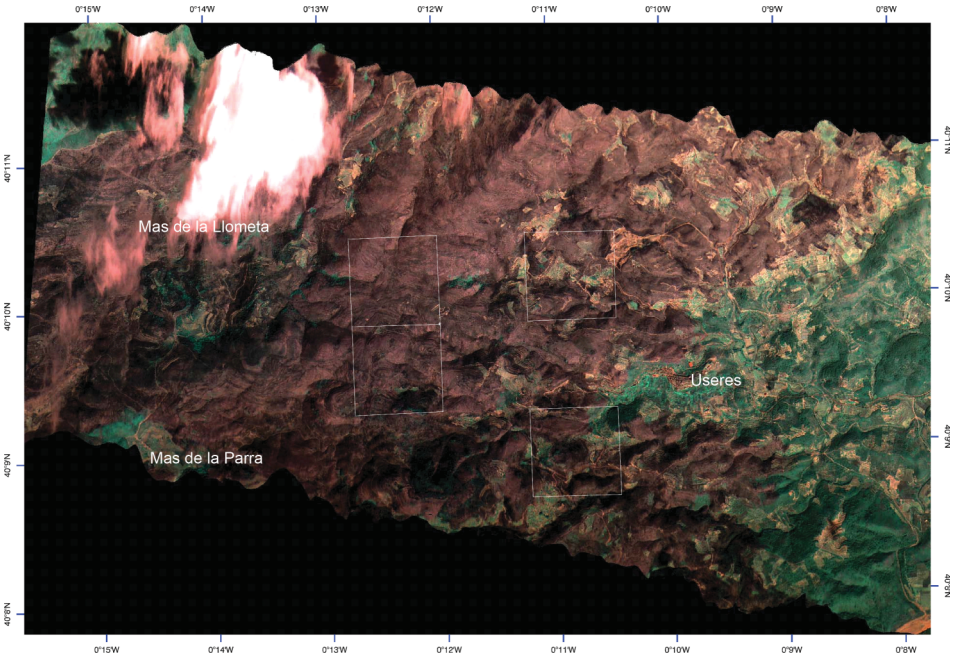

Figure 5. AHS image of the burnt area, RGB composition (bands 5–13–18). Burnt area is coloured in brown, and white squares mark selected pixels.

Those classifications were considered as a reference, and we used them to quantify percentages of use per class, and compared them with the corresponding AVHRR pixel. Table 2 shows percentage covered by each class in the four pixels. Pixel 2 (top left) seems to be more affected by fire with a maximum span of burnt area of 99.8%, though part of this percentage corresponds to burnt area with some vegetation patches (37.7%).

The pixel with the most totally burnt area is 1, with 48.2% of its area completely burnt. Nearly 20% of this pixel could preserve part of its original vegetation, most of it within the southern part of the image and near the border of the area affected by fire (see figure 6 bottom left). Pixels 3 and 4 (figure 6, top right and bottom right, respectively) have a larger area of unaffected vegetation (25% and 26%, respectively), but they also have a large burnt area, and some other land covers, such as rock and

Table 2. Percentage area covered by land classes per pixel.

Classes	Pixel 1 (%)	Pixel 2 (%)	Pixel 3 (%)	Pixel 4 (%)
Vegetation (VEG)	18.97	0.19	25.11	26.10
Shadowed vegetation (VEGS)	4.12	–	–	–
Burnt (BUR)	48.19	30.28	36.41	41.64
Shadowed burnt (BUS)	11.24	10.45	18.27	11.80
Mixed vegetation burnt (VEB)	–	12.76	–	14.02
Burnt with vegetation patches (BUV)	–	37.70	4.63	–
Rocks and bare soils (ROC)	17.3	8.62	15.58	6.43
Total burnt (excluding VEG and VEGS)	76.73	99.81	74.90	73.90

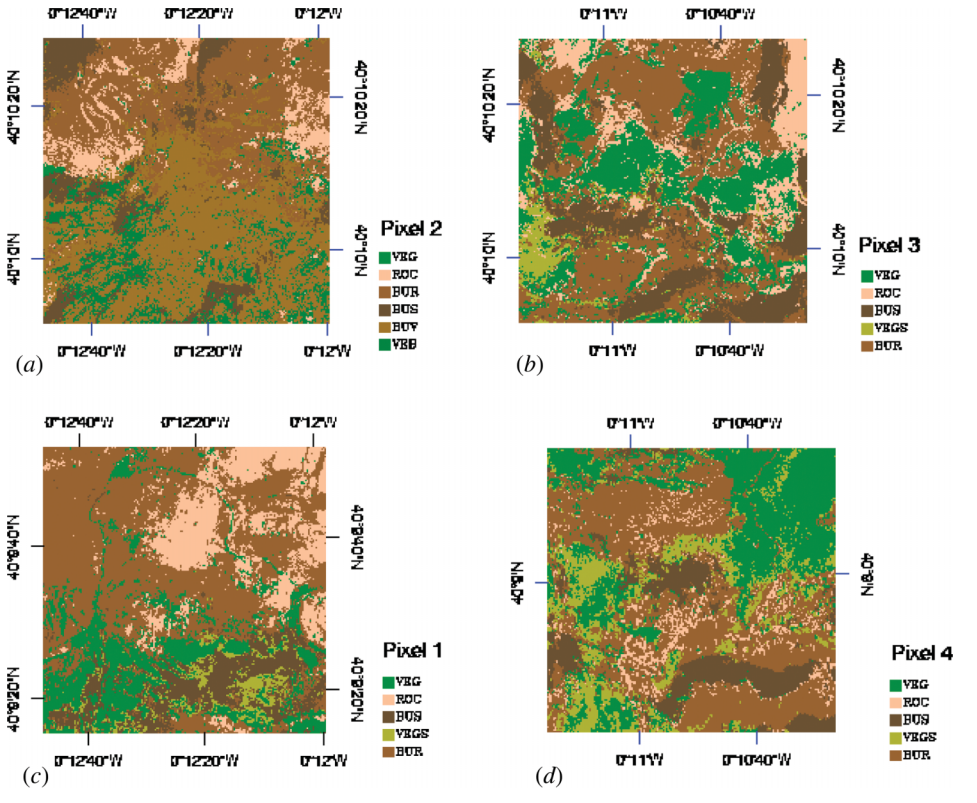

Figure 6. Classifications of AHS pixels: healthy vegetation (VEG), shadowed vegetation (VEGS), burnt area (BUR), burnt area in shadow (BUS), partly burnt vegetation (VEB), burnt area with small vegetation patches (BUV) and rocks and bare soil (ROC). Identification of pixels is as follows: (*a*) pixel 2, (*b*) pixel 3, (*c*) pixel 1 and (*d*) pixel 4.

bare soil (16% in pixel 3 and 7% in pixel 4). If we calculate a mean value (not shown in table 2), more than 50% of the total area covered by the four pixels has burnt completely, plus 30% more, included as burnt area, is composed of patches of burnt and unburnt zones with a significant part of bare soil where it is more difficult to determine the severity of the fire. We decided to reclassify rocks and bare soil as burnt in the pixel classifications because they negatively affect the NDVI and they also turned darker after the fire. Therefore, they are included as burnt area in the AVHRR data as well.

A minimum error related with different scales and georeferencing issues has also been calculated. Location of one of the classified pixels (pixel 3) was moved half an AVHRR pixel in each direction (500 m) and was again classified in each new position to achieve percentages of burnt and vegetation areas (see figure 7). Pixel 3 was chosen because it covers a more heterogeneous area and also because moving the pixel in four directions could be problematic if using any of the other 3 pixels due to the extent of the AHS image (see figure 5). The average of the burnt area for the 4 pixels is 76%, and 24% is assigned to vegetation (see table 3 for details).

If we compare these results with percentages of pixel 3 where burnt area is near 75% of the terrain, we can conclude that, even when there must be some minimum error

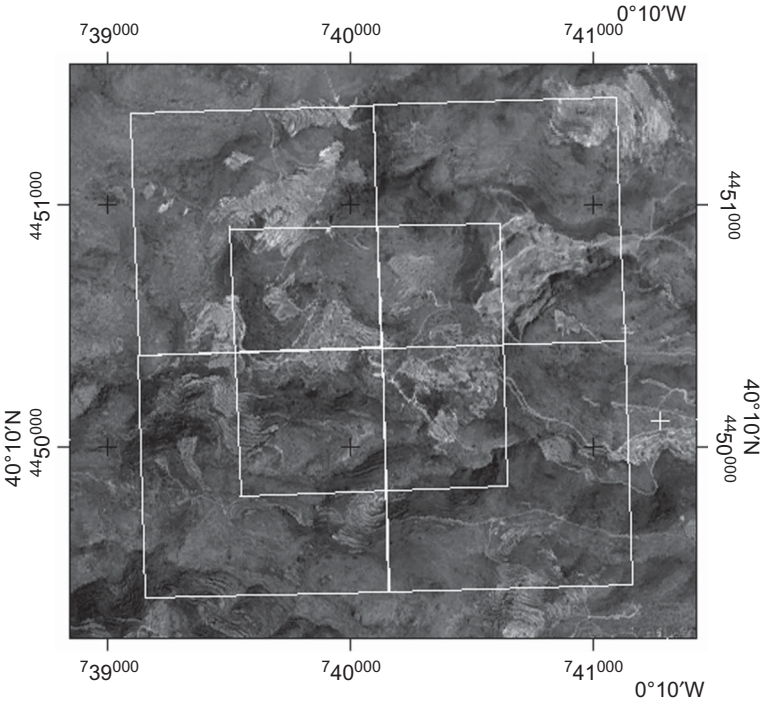

Figure 7. Validation of estimated percentage of pixel 3 by moving its location 500 m in each direction (half of an AVHRR pixel).

Table 3. Percentage area covered by land classes in test pixel 3.

Classes	Pixel 3 TR(%)	Pixel 3 BR (%)	Pixel 3 BL(%)	Pixel 3 TL(%)	Mean (%)
Vegetation	15	23	34	25	24
Burnt	85	77	66	75	76

TR: top right, BR: bottom right, LB: bottom left, TL: top left.

related to the different spatial resolutions, results remain coherent. The comparison between the map obtained from the AVHRR and ground-truth percentages from the AHS is shown in table 4. The results show an average error of 6.5%, with a maximum deviation of 17% and a minimum of 1%. The results confirm that the AVHRR confidently approximates sub-pixel burnt area in spite of its low spatial resolution.

Table 4. Results of the AHS classification versus the AVHRR classification of burnt areas.

	Pixel 1(%)	Pixel 2(%)	Pixel 3(%)	Pixel 4(%)	Mean (%)
AVHRR	78	93	92	89	88
AHS	77	100	75	74	81.50
Error difference	1	–7	17	15	6.50

5. Discussion

SMA techniques can be successful if appropriate endmember selection is made. Selection of endmembers starts by identifying the number of them to be used in the SMA and their corresponding spectral signatures. Sometimes, the use of only two endmembers can underestimate the model (Theresia *et al.* 2003). In some references that use Landsat Thematic Mapper (TM) / Enhanced Thematic Mapper Plus (ETM+), three or more endmembers were selected to represent the whole variability of the scene (Ridd 1995, Radeloff *et al.* 1999, Small 2001). In the present work, we carried out different tests using two endmembers selected from an NDVI image, and we compared the results with a procedure that used all pixels in the NDVI image as endmembers in an iterative process. There is clear evidence that the use of a larger number of endmembers increases the accuracy of the results.

The SMA approach used here works similarly to that developed by Roberts *et al.* (1998), where they developed a multiple endmember spectral mixture analysis (MESMA) to map sub-pixel proportion. The main variation in our method is that we did not use the spectral signatures to proceed with the unmixing analysis, but two products that were derived from the spectral data, the NDVI and the LST. This introduces a considerable modification of the unmixing produced because the linearity of the method is lost when using these two different parameters. However, NDVI and LST have been shown to present a linear correlation depending on land-cover characteristics (Nemani *et al.* 1993, Hope *et al.* 2005, Yue *et al.* 2007) and to be related to surface-moisture status (Sandholt *et al.* 2002), which makes them appropriate parameters in an unmixing analysis of this type. Moreover, Julien and Sobrino (2009) showed that a linear relation between NDVI and LST could be evidenced for most biomes, since the presence of vegetation (estimated through the NDVI parameter) tends to decrease surrounding temperatures, air temperature as well as LST, through the mechanism of evapotranspiration (Lambin and Ehrlich 1996). Therefore, a decrease in NDVI values after the fire can be related to an increase in the LST values and vice versa. However, the use of both parameters is not redundant, due to the low values of NDVI for sparsely vegetated areas such as the study area.

Use of the AVHRR is due to opportunity and easy access, both requirements that are fundamental in a rapid response to hazardous events. One possible extension of the work on this feature could be testing our approach on other types of multi-spectral data with a higher resolution, such as the MODIS or even Landsat ETM+.

6. Conclusion

AVHRR images are commonly used for a great variety of environmental studies, including fire detection. However, the low spatial resolution of the sensor can limit the accuracy of some measurements, and in these cases, it is necessary to have ancillary data to help with the interpretation of the parameters of interest. We have presented here a new method that uses the MSMA technique with NDVI and LST as input data in the unmixing procedure. We have applied it to a particular fire case in a small area in the province of Castellon called L'Alcalaten. The results of total-area estimation using this methodology showed an average result of 54 ± 1 burnt km^2 using the two end dates, corroborating the official estimations of the MMA (57 km^2). The percentile map of the area burnt per pixel agreed with the ground-truth data, obtained by means of applying a supervised classification procedure of an AHS image, with a mean error of less than 7%. The results obtained are encouraging, and they show good agreement

between both maps. Our conclusion is that the MSMA technique applied to the AVHRR data can be used with confidence to give approximate results of sub-pixel burnt area prior to the use of finer spatial-resolution sensors by using a relatively simple method of SMA. Considering the fact that the AVHRR is a sensor used for a broad community of remote-sensing researchers and its images can be relatively easy to acquire and process, our simple method can contribute to the study of fire events with high accuracy in conjunction with ancillary high-spatial- and high-spectral-resolution data.

Acknowledgements

We would like to thank the ESA for contributing with the CEFLES project and the Spanish Ministry of Education for the TERMASAT project. This work was also supported in part by the Generalitat Valenciana by means of the grants for post-doctoral researches in centres of the Comunidad Valenciana. The authors would like to thank the Ministry of Environment, especially J. Merida for his kind answers to our needs. We would also like to thank the European Union for EAGLE, project SST3-CT-2003-502 057.

References

Asner, G.P., Wessman, C.A. and Privette, J.L, 1997, Unmixing the directional reflectances of AVHRR sub-pixel land covers. *IEEE Transaction in Geoscience and Remote Sensing*, **35**, pp. 868–878.

Atkinson, P.M., Cutler, M.E.J. and Lewis, H., 1997, Mapping sub-pixel proportional land cover with AVHRR imagery. *International Journal of Remote Sensing*, **18**, pp. 917–935.

Barbosa, P.M., Cardoso Pereira, J.M. and Gregoire, J.M., 1998, Compositing criteria for burnt area assessment using multitemporal low resolution satellite data. *Remote Sensing of Environment*, **65**, pp. 38–49.

Barbosa, P.M., Gregoire, J.M. and Cardoso Pereira, J.M., 1999, An algorithm for extracting burnt areas from time series of AVHRR GAC data applied at a continental scale. *Remote Sensing of Environment*, **69**, pp. 253–263.

Carpenter, G.H., Gopal, S., Macomber, S., Martens, S. and Woodcock, C.E., 1999, A neural network method for mixture estimation for vegetation mapping. *Remote Sensing of Environment*, **70**, pp. 138–152.

Chuvieco, E., Englefield, P., Trischenko, A.P. and Luo, Y., 2008, Generation of long time series of burn area maps of the boreal forest from NOAA-AVHRR composite data. *Remote Sensing of Environment*, **112**, pp. 2381–2396.

Congalton, R. and Green, K., 1999, *Assessing the Accuracy of Remotely Sensed Data: Principles and Practices* (Boca Raton, FL: CRC/Lewis Press).

Coppin, P., Jonckheere, I., Nackaerts, K., Muys, B. and Lambin, E., 2004, Digital change detection methods in ecosystem monitoring: a review. *International Journal of Remote Sensing*, **25**, pp. 1565–1596.

Cross, A.M., Settle, J.J., Drake, N.A. and Paivinen, R.T.M., 1991, Sub-pixel measurement of tropical forest cover using AVHRR data. *International Journal of Remote Sensing*, **12**, pp. 1119–1129.

Defries, R.S., Hansen, M.C. and Townshend, J.R.G., 2000, Global continuous fields of vegetation characteristics: a linear mixture model to multi-layer 8 km AVHRR data. *International Journal of Remote Sensing*, **21**, pp. 1389–1414.

Elmore, A.J., Mustard, J.F., Manning, S.J. and Lobell, D.B., 2000, Quantifying vegetation change in semiarid environments: precision and accuracy of spectral mixture analysis and the NDVI. *Remote Sensing of Environment*, **73**, pp. 87–102.

GILLESPIE, A.R., 1992, Spectral mixture analysis of multispectral thermal infrared images. *Remote Sensing of Environment*, **42**, pp. 137–145.

HOLBEN, B.N. and SHIMABUKURO, Y.E., 1993, Linear mixing model applied to coarse spatial resolution data from multispectral satellite sensors. *International Journal of Remote Sensing*, **14**, pp. 2231–2240.

HOPE, A., ENGSTROM, R. and STOW, D., 2005, Relation between AVHRR surface temperature and NDVI in Arctic tundra ecosystems. *International Journal of Remote Sensing*, **26**, pp. 1771–1776.

JULIEN, Y. and SOBRINO, J.A., 2009, The yearly land cover dynamics (YLCD) method: an analysis of global vegetation from NDVI and LST parameters. *Remote Sensing of Environment*, **113**, pp. 329–334.

KERDILES, H. and GRONDONA, M.O., 1995, NOAA-AVHRR NDVI decomposition and subpixel classification using linear mixing in the Argentinean Pampa. *International Journal of Remote Sensing*, **16**, pp. 1303–1325.

LAMBIN, E.F. and EHRLICH, D., 1996, The surface temperature-vegetation index space for land cover and land-cover change analysis. *International Journal of Remote Sensing*, **17**, pp. 163–487.

MINISTERIO DE MEDIO AMBIENTE (MMA), 2008, Los incendios forestales en España año 2007. Available online at: http://www.mma.es/secciones/biodiversidad/defensa_incendios/estadisticas_incendios/pdf/incendios_forestales_espania_2007.pdf (18 August 2010).

NEMANI, R., PIERCE, L., RUNNING, S. and GOWARD, S., 1993, Developing satellite-derived estimates of surface moisture status. *Journal of Applied Meteorology*, **32**, pp. 548–557.

POZO, D., OLMO, F.J. and ALADOS-ARBOLEDAS, L., 1997, Fire detection and growth monitoring using a multitemporal technique on AVHRR mid-infrared and thermal channels. *Remote Sensing of Environment*, **60**, pp. 111–120.

QUINTANO, C., FERNÁNDEZ-MANSO, A., FERNÁNDEZ-MANSO, O. and SHIMABUKURO, Y.E., 2006, Mapping burnt areas in Mediterranean countries using spectral mixture analysis from a uni-temporal perspective. *International Journal of Remote Sensing*, **27**, pp. 645–662.

RADELOFF, V.C, MLADENOFF, D.J. and BOYCE, M.S., 1999, Detecting Jack pine budworm defoliation using spectral mixture analysis: separating effects from determinants. *Remote Sensing of Environment*, **69**, pp. 156–169.

RIDD, M.K., 1995, Exploring a V-I-S (vegetation-impervious surface-soil) model for urban ecosystem analysis through remote sensing: comparative anatomy for cities. *International Journal of Remote Sensing*, **16**, pp. 2165–2185.

ROBERTS, D.A., BATISTA, G.T., PEREIRA, J., WALLER, E.K. and NELSON, B.W., 1998, Change identification using multitemporal spectral unmixing analysis: applications in eastern Amazonia. In *Remote Sensing Change Detection: Environmental Monitoring Applications and Methods*, C. Elvidge and R. Lunetta (Eds), pp. 137–161 (Ann Arbor, MI: Ann Arbor Press).

SANDHOLT, I., RASMUSSEN, K. and ANDERSEN, J., 2002, A simple interpretation of the surface temperature/vegetation index space for assessment of surface moisture status. *Remote Sensing of Environment*, **79**, pp. 213–224.

SAUNDERS, R.W. and KRIEBEL, K.T., 1998, An improved method for detecting clear sky and cloudy radiances from AVHRR data. *International Journal of Remote Sensing*, **9**, pp. 123–150.

SMALL, C., 2001, Estimation of urban vegetation abundance by spectral mixture analysis. *International Journal of Remote Sensing*, **22**, pp. 1305–1334.

SOBRINO, J.A. and RAISSOUNI, N., 2000, Towards remote sensing methods for land cover dynamic monitoring: application to Marocco. *International Journal of Remote Sensing*, **21**, pp. 353–363.

SONG, C., 2005, Spectral mixture analysis for subpixel vegetation fractions in the urban environment: how to incorporate endmember variability? *Remote Sensing of Environment*, **95**, pp. 248–263.

Sousa, A.M., Pereira J.M.C. and Silva, J.M.N., 2003, Evaluating the performance of multi-temporal image compositing algorithms for burnt area analysis. *International Journal of Remote Sensing*, **24**, pp. 1219–1236.

Theresia, M.A., Thomas, G., Taylor, J.C., Gemmell, F. and Varjo, J., 2003, Sensitivity of mixture modelling to endmember selection. *International Journal of Remote Sensing*, **24**, pp. 1559–1575.

Yue, W., Xu, J., Tan, W. and Xu, L., 2007, The relationship between land surface temperature and NDVI with remote sensing: application to Shanghai Landsat 7 ETM+ data. *International Journal of Remote Sensing*, **28**, pp. 3205–3226.